
Evaluation of ^{18}F -FDG PET in Patients with Advanced, Metastatic, or Recurrent Gastric Cancer

Takashi Yoshioka, MD¹; Keiichirou Yamaguchi, MD^{2,3}; Kazuo Kubota, MD²; Toshiyuki Saginoya, MD³; Tetsuro Yamazaki, MD⁴; Tatuio Ido, PhD³; Gengo Yamaura, MD¹; Hiromu Takahashi, MD¹; Hiroshi Fukuda, MD²; and Ryunosuke Kanamaru, MD¹

¹Department of Clinical Oncology, Institute of Development, Aging and Cancer, Tohoku University, Sendai, Japan;

²Department of Nuclear Medicine and Radiology, Institute of Development, Aging and Cancer, Tohoku University,

Sendai, Japan; ³Cyclotron and Radioisotope Center, Tohoku University, Sendai, Japan; and ⁴Department of

Diagnostic Radiology, Tohoku University Hospital, Tohoku University, Sendai, Japan

PET with ^{18}F -FDG has been widely used in oncology, but its application for stomach neoplasms has been limited. The aim of this study was to evaluate the visual diagnostic accuracy of ^{18}F -FDG PET for advanced, metastatic, or recurrent gastric cancer and to generate semiquantitative values for lesions.

Methods: ^{18}F -FDG PET scans were obtained on 42 patients (29 men, 13 women; age, 27–78 y; median age, 63 y): 20 patients with a PT931/04 scanner and 22 patients with a SET2400W scanner. The PT931/04 has a spatial resolution of 6.0 mm at full width at half maximum (FWHM) and covers 15 cm above and below the targeted lesion, and the SET2400W has a spatial resolution of 3.9 mm at FWHM and images the entire body. All PET images were interpreted visually, and tracer uptakes were quantitated as standardized uptake values (SUVs) on SET2400W images. **Results:** The sensitivity, specificity, and accuracy as a whole were as follows: 71%, 74%, and 73%, respectively, with the SET2400W scanner and 47%, 79%, and 62%, respectively, with the PT931/04 scanner. Values were high for primary lesions, liver, lymph node, and lung metastases, but were low for bone metastases, ascites, peritonitis, and pleuritis carcinomatosa. SUVs were 8.9 ± 4.2 (primary lesions, 19 patients/19 lesions), 6.5 ± 2.2 (liver, 9/55), 6.1 ± 2.5 (lymph nodes, 14/38), 6.5 ± 1.8 (abdominal wall, 4/7), 3.9 ± 2.0 (bone, 3/27), and 4.7 ± 2.6 (lung, 2/3). Comparing SUVs and histologic findings for 17 untreated patients, values for well-differentiated and moderately differentiated adenocarcinomas versus poorly differentiated adenocarcinomas and signet ring cell carcinomas were 13.2 ± 6.3 (4/4) versus 7.7 ± 2.6 (13/13) ($P < 0.05$) for the primary lesions, 7.0 ± 2.4 (5/39) versus 5.6 ± 2.8 (2/2) for the liver, and 5.5 ± 1.9 (9/28) versus 8.8 ± 3.3 (3/8) ($P < 0.05$) for the lymph nodes. **Conclusion:** Our results indicate that ^{18}F -FDG PET is a useful diagnostic modality for advanced, metastatic, or recurrent gastric cancer but not for detecting bone metastases, peritonitis, or pleuritis carcinomatosa. ^{18}F -FDG uptake by gas-

tric cancers is relatively high but does not parallel histopathologic features of malignancy.

Key Words: PET; ^{18}F -FDG; gastric cancer

J Nucl Med 2003; 44:690–699

Gastric cancer continues to be the most common malignancy in Japan. The development of diagnostic modalities and surgical techniques has improved the prognosis, but associated mortality is still the second highest, next to lung cancer (1). This is due to stage IV and postoperative recurrent cancers and, therefore, it is very important to develop effective treatments, especially chemotherapy. In clinical practice, success depends on the choice of adequate chemotherapeutic agents and it is essential to monitor their efficacy in a decision-making process.

PET with ^{18}F -FDG is a noninvasive approach for determination of the glycolytic status. PET is able to make an image that shows the tissue distribution of the positron emitter, ^{18}F -FDG being a structural analog of glucose labeled with the short-lived positron-emitting ^{18}F (2). ^{18}F -FDG is transported into the cell via a glucose-transporter and then is converted to ^{18}F -FDG-6-phosphate by hexokinase in cells. However, it is not a substrate for further metabolism nor is it permeable to the cell membrane; therefore, it accumulates within the cell (3). Enhanced glycolysis is one of the most important characteristics of cancer cells (4), and ^{18}F -FDG PET has proven to be successful for imaging various malignant neoplasms (5–16).

^{18}F -FDG PET can serve as a diagnostic instrument for follow-up after cancer treatment because it indicates the viability of the tumor cells (17). Response to radiotherapy or chemotherapy is recordable earlier and more exactly in terms of ^{18}F -FDG accumulation than by morphologic changes (18,19); in fact, ^{18}F -FDG PET has been found to have wide application for treatment evaluation of malignant

Received Aug. 16, 2002; revision accepted Dec. 19, 2002.

For correspondence or reprints contact: Takashi Yoshioka, MD, Department of Clinical Oncology, Institute of Development, Aging and Cancer, Tohoku University, 4-1, Seiryomachi, Aoba-ku, Sendai 980-8575, Japan.

E-mail: ytakashi@idac.tohoku.ac.jp

tumors (20–23). However, information on its use for gastric cancer is limited (24–27), especially regarding advanced, metastatic, or recurrent cases (28).

The purpose of this study was to evaluate the clinical usefulness of ¹⁸F-FDG PET in a series of patients with advanced gastric cancers and to prepare a basis for using this modality to monitor the efficacy of chemotherapy.

MATERIALS AND METHODS

Patients

Between December 1986 and September 2001, 42 patients (29 men, 13 women; age, 27–78 y; mean age, 59.2 y) with advanced, metastatic, or recurrent gastric cancers were studied with ¹⁸F-FDG PET. Thirty-six patients had biopsy-proven malignancies with sampling of primary lesions and 6 had histologically proven ma-

TABLE 1
Patient Characteristics, with Macroscopic Classification, Histology, and Metastatic Sites and Treatment Before PET

Scanner	Patient	Age (y)	Sex	Primary (Borrmann)	Histology	Metastases	Chemotherapy before PET	Recent surgery
PT931/04	E01	72	F	IV	Sig	Liver, Lym (abd)	Yes	
	E02	62	M	III	Well	Liver, Lym (abd), PC, ascites	Yes	
	E03	72	M	No	Poor	Liver, PC, ascites	No	
	E04	78	M	III	Mod	Lym (abd)	Yes	
	E05	69	M	III	Poor	Liver, Lym (abd)	No	
	E06	35	F	IV	Poor	PC	No	Exp
	E07	56	M	III	Mod	Liver, Lym (abd), PC, ascites	Yes	
	E08	60	M	No	Mod	Liver	Yes	
	E09	50	M	III	Well	Lym (abd)	Yes	
	E10	63	M	No	Muc	Liver	Yes	
	E11	78	M	IV	Poor	Lym (abd)	Yes	
	E12	45	F	II	Sig	PC, ascites	Yes	
	E13	60	F	IV	Sig	PC, ascites	No	Exp
	E14	35	M	IV	Poor	PC, ascites	No	
	E15	62	F	IV	Poor	No	No	
	E16	46	M	IV	Mod	Liver, Lym (abd)	No	
	E17	63	F	III	Sig	Lym (abd)	No	
	E18	66	M	III	Mod	Liver, Lym (abd), PC, ascites	No	
	E19	76	M	III	Mod	Liver, Lym (abd)	Yes	
	E20	71	F	I	Well	PC, ascites	Yes	
SET2400W	S01	68	M	II	Well	Liver, Lym (abd)	Yes	
	S02	69	M	III	Poor	Lym (abd)	No	
	S03	42	M	No	Sig	PC	Yes	Ileus
	S04	66	M	III	Poor	Liver, Lym (abd)	No	
	S05	63	M	III	Well	Lung, PC, ascites	No	
	S06	69	M	II	Poor	Liver, Lym (abd)	No	
	S07	49	M	III	Poor	Liver, Lym (abd), bone (cost)	No	
	S08	27	F	V	Sig	PC, ascites	No	
	S09	42	F	No	Poor	PC, ascites, PIC	No	
	S10	64	M	III	Mod	Lym (abd)	No	
	S11	69	M	III	Poor	Liver, Lym (abd), PC	Yes	Bypass
	S12	72	M	No	Mod	PC (schnitzuler)	No	Ileus
	S13	48	M	I	Poor	No	No	
	S14	59	M	IV	Sig	PC, ascites	No	Exp
	S15	34	F	V	Sig	Lym (abd, Virchow), PC, ascites, PIC	No	
	S16	74	M	II	Poor	Liver, Lym (abd, mediastinal), Lung, PC, ascites, PIC	No	
	S17	64	F	II	Well	Liver, Lym (abd)	No	Bypass
	S18	61	M	I	Poor	No	No	
	S19	63	M	II	Mod	Liver, Lym (abd), PIC	No	
	S20	73	M	III	Poor	Liver, Lym (abd, Virchow), PC, ascites, bone (multiple)	No	
	S21	41	F	V	Poor	Lym (abd), bone (multiple)	No	
	S22	52	M	III	Poor	Lym (abd)	No	

Sig = signet ring cell carcinoma; Lym = lymph node metastasis; abd = abdomen; Well = well-differentiated adenocarcinoma; PC = peritonitis carcinomatosis; Poor = poorly differentiated adenocarcinoma; Mod = moderately differentiated adenocarcinoma; Exp = exploratory laparotomy; Muc = mucinous adenocarcinoma; Ileus = operation to relieve ileus status; cost = costae; PIC = pleuritis carcinomatosis; Bypass = gastrointestinal bypass.

lignancies from prior surgical excision of the primary tumors. Of the total, 28 patients had no prior chemotherapy, including 3 after exploratory laparotomy and 1 after gastrointestinal bypass. A total of 14 patients had prior chemotherapy but, in all cases, they were studied >4 wk after the prior chemotherapy and just before a new regimen because the prior regimen had failed. One patient underwent surgery to relieve an ileus state 4 wk before ¹⁸F-FDG PET, which was caused by peritonitis carcinomatosa during chemotherapy. Another patient underwent gastrointestinal bypass surgery 4 wk before ¹⁸F-FDG PET because he had ascites but this disappeared with chemotherapy. There were no diabetic patients. Patient characteristics are presented in Table 1.

All patients underwent physical examination, ultrasonography, double-contrast barium radiography, upper endoscopy, and CT within 2 wk before ¹⁸F-FDG PET. CT scans were obtained on the upper abdomen of all patients and in the range from the neck to the pelvis for those undergoing whole-body PET. Bone scintigraphy (*n* = 3) was performed when clinically indicated. Cytology was performed when ascites or pleural effusion existed and samples could be collected. All patients were monitored by physical examinations, upper endoscopy, ultrasonography, and CT after ¹⁸F-FDG PET for >4 mo, every 1 or 2 mo, except for 1 patient who died within 1 mo of ¹⁸F-FDG PET.

The study protocol was approved by the Ethics Committee for Clinical Research of Tohoku University and informed consent was obtained from each patient.

Radiopharmaceuticals

¹⁸F-FDG was synthesized using an automated synthesis system by the method described by Shiue et al. (29). Radiochemical purity was >99%. Quality assurance tests for clinical use were performed according to the safety guidelines of our university. The mean injected dose of ¹⁸F-FDG was 222 ± 72 MBq (range, 103–400 MBq) (2.8–10.8 mCi).

PET

All patients fasted for at least 4 h before PET, and blood glucose levels were measured before injection of ¹⁸F-FDG. PET scans were obtained using a PT931/04 scanner (Siemens-CTI, Knoxville, TN) from 1986 to 1996 (20 patients) and a SET2400W scanner (Shimadzu Inc., Kyoto, Japan) from 1996 onward (22 patients).

The PT931/04 scanner provides seven 7.15-mm-wide slices, featuring simultaneous acquisition with a 50-mm axial field of view, a spatial resolution of 6.0 mm at full width half maximum (FWHM), and a sensitivity per slice of 157 kilocounts/second (kcps)/MBq/mL (30). A CT scan was obtained and a line indicating the site of the targeted lesion was drawn 1 d before ¹⁸F-FDG PET. After transmission scanning was performed for 10–15 min with a ⁶⁸Ge/⁶⁸Ga ring source for attenuation correction, emission imaging was performed in one 7.5- to 10-min frame above the drawn line and 1 or 2 frames below the line, beginning 30 min after injection of ¹⁸F-FDG. Axial PET images were reconstructed after correction for dead time, decay, and photon attenuation.

The SET2400W scanner acquires 66 planes simultaneously over a 200-mm axial field of view with a spatial resolution of 3.9 mm at FWHM and a sensitivity per slice of 97 kcps/MBq/mL (31). Emission scans were obtained from head to thigh for 5 min per frame, 45 min after injection of ¹⁸F-FDG. A transmission scan was obtained for 5 min per frame with the ⁶⁸Ge/⁶⁸Ga ring source for attenuation correction after the emission scan. PET images were reconstructed using measured attenuation, dead time, and decay correction factors.

Visual Analysis

Qualitative evaluation of PET scans was performed blinded and independently by 3 PET specialists with images from the patients with gastric cancers but without knowledge of any other clinical information.

Most of the image data obtained by the PT931/04 and all data obtained by the SET2400W were converted to the analysis format with special software packages, adjusting the cross-calibration factors between PT931/04 and SET2400W. The calibration factors were calculated on both machines twice every month, and we converted the analysis formats to the standardized uptake value (SUV = activity concentration/injected dose per body weight) images with the window range of 0–5 for the SUV, using each calibration factor and the patient's body weight. Hard copies of consecutive transaxial sections with a linear gray scale were printed out using the image data from the PT931/04. The image data from the SET2400W proceeded to the process of transaxial and coronary 12-mm reslices, and hard copies of consecutive transaxial and coronary sections covering from the top of the head to the thigh were printed out with a linear gray scale.

The following parameters were evaluated: visibility of the primary lesion; presence of liver and lymph node metastases; and presence of ascites and peritonitis carcinomatosa in images from the PT931/04 and SET2400W and presence of lung and bone metastases and pleuritis carcinomatosa in images from the SET2400W. The lesions were designated as positive (P), questionably positive (QP), negative (N), or questionably negative (QN). The accumulations were assigned QP when they were thought to be malignant but the possibility of physiologic accumulations could not be ruled out; they were assigned QN when they were thought to be physiologic but the possibility of the malignancy could not be ruled out. Questionnaires involving all items and figures for the whole body were prepared. If there were other findings in addition to the items or multiple lesions for liver, lymph nodes, lung, and bone metastases, each was added to the figure and evaluated.

The gold standards used for verifying lesion malignancy were as follows: upper endoscopy for primary lesions; CT and clinical course for liver, lymph node and lung metastases; CT, cytology, and clinical course for ascites, peritonitis carcinomatosa, and

TABLE 2
Numbers of Patients with Primary Lesions and Metastases, PC, PIC, or Ascites

Primary lesions or metastases	No. of patients (no. of lesions)	
	PT931/04	SET2400W
Prim	17	19
Liver	10 (40)	9 (55)
Lym	11 (20)	14 (38)
Lung		2 (3)
PC	9	10
Ascites	8	7
PIC		4
Bone		3 (27)

Prim = primary lesions; Liver = liver metastases; Lym = lymph node metastases; Lung = lung metastases; PC = peritonitis carcinomatosa; PIC = pleuritis carcinomatosa; Bone = bone metastases.

TABLE 3

Sensitivity, Specificity, and Accuracy of ¹⁸F-FDG PET Overall and for Each Separate Lesion on Visual Analysis

Scanner	Overall	Prim	Liver	Lym	Lung	PC	Ascites	PIC	Bone
PT931/04									
Sensitivity (%)	47	70	78	47		9	2		
Specificity (%)	79	78	82	62		79	93		
Accuracy (%)	62	71	80	54		48	57		
SET2400W									
Sensitivity (%)	71	91	85	73	67	50	24	4	30
Specificity (%)	74	100	74	78	88	63	76	100	82
Accuracy (%)	73	92	79	75	86	57	59	83	57

Overall = all lesions; Prim = primary lesions; Liver = liver metastases; Lym = lymph node metastases; Lung = lung metastases; PC = peritonitis carcinomatosis; PIC = pleuritis carcinomatosis; Bone = bone metastases.

PT931/04 scanner has spatial resolution of 6.0 mm at FWHM and sensitivity per slice of 157 kcps/MBq/mL. SET2400W scanner has spatial resolution of 3.9 mm at FWHM and sensitivity per slice of 97 kcps/MBq/mL.

pleuritis carcinomatosis; ^{99m}Tc-methylene diphosphonate (^{99m}Tc-MDP) bone scintigraphy and clinical course for bone metastases. "Clinical course" means all of the follow-up examinations and autopsies. Suspected lesions were compared between the initial and follow-up examinations and were designated as actual lesions chiefly on the basis of change of sizes. The number of lesions was counted individually. If the lesions were clumped or could not be divided, they were counted as a single lesion.

Sensitivity, specificity, and accuracy were calculated on the basis of the results of visual analysis. QP and QN were dealt with by having the importance to each side of trueness and falseness set at half and half, and the following equations were used:

$$\text{True-Positive (TP)} = P(+) + 0.5 \times QP(+),$$

$$\text{False-Positive (FP)} = P(-) + QP(-) + 0.5 \times QN(-),$$

$$\text{False-Negative (FN)} = N(+) + QN(+) + 0.5 \times QP(+),$$

$$\text{True-Negative (TN)} = N(-) + 0.5 \times QN(-),$$

where P(+) = P in the presence of a malignant lesion, P(-) = P in the absence of a malignant lesion, QP(+) = QP in the presence of a malignant lesion, QP(-) = QP in the absence of a malignant lesion, N(+) = N in the presence of a malignant lesion, and N(-) = N in the absence of a malignant lesion.

$$\text{Sensitivity (\%)} = TP \div (TP + FN) \times 100.$$

$$\text{Specificity (\%)} = TN \div (TN + FP) \times 100.$$

$$\text{Accuracy (\%)} = (TP + TN) \div (TP + TN + FP + FN) \times 100.$$

For discrimination of malignant lesions in patients with gastric cancer on PET, a receiver operating characteristic (ROC) curve of

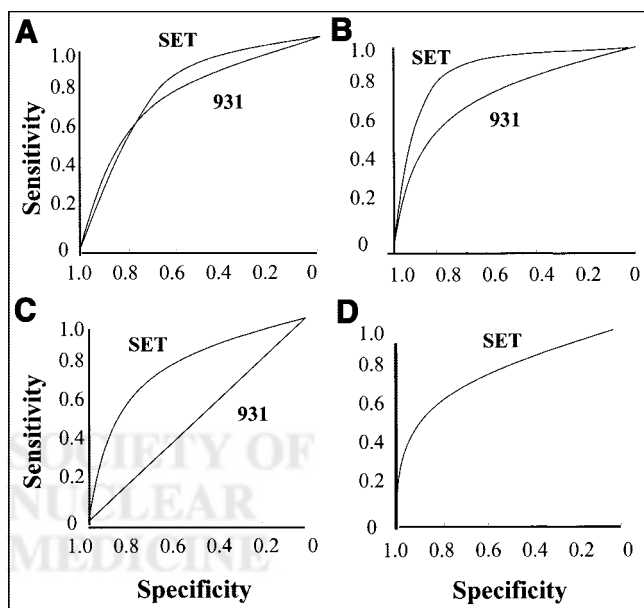


FIGURE 1. ROC curves for sites of primary lesions (A), liver (B), lymph node (C), and lung (D) metastases. SET = SET2400W; 931 = PT931/04. Each curve reflects high detectability of these lesions.

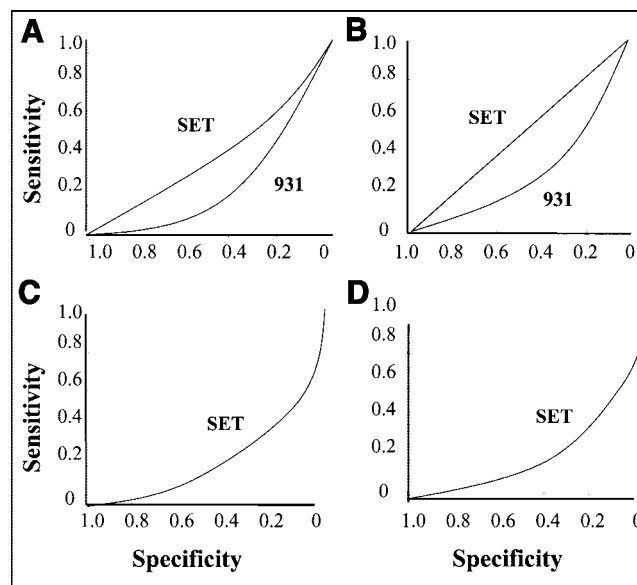


FIGURE 2. ROC curves for lesions of peritonitis carcinomatosis (A), ascites (B), pleuritis carcinomatosis (C), and bone metastases (D). SET = SET2400W; 931 = PT931/04. Each curve reflects low detectability of these lesions.

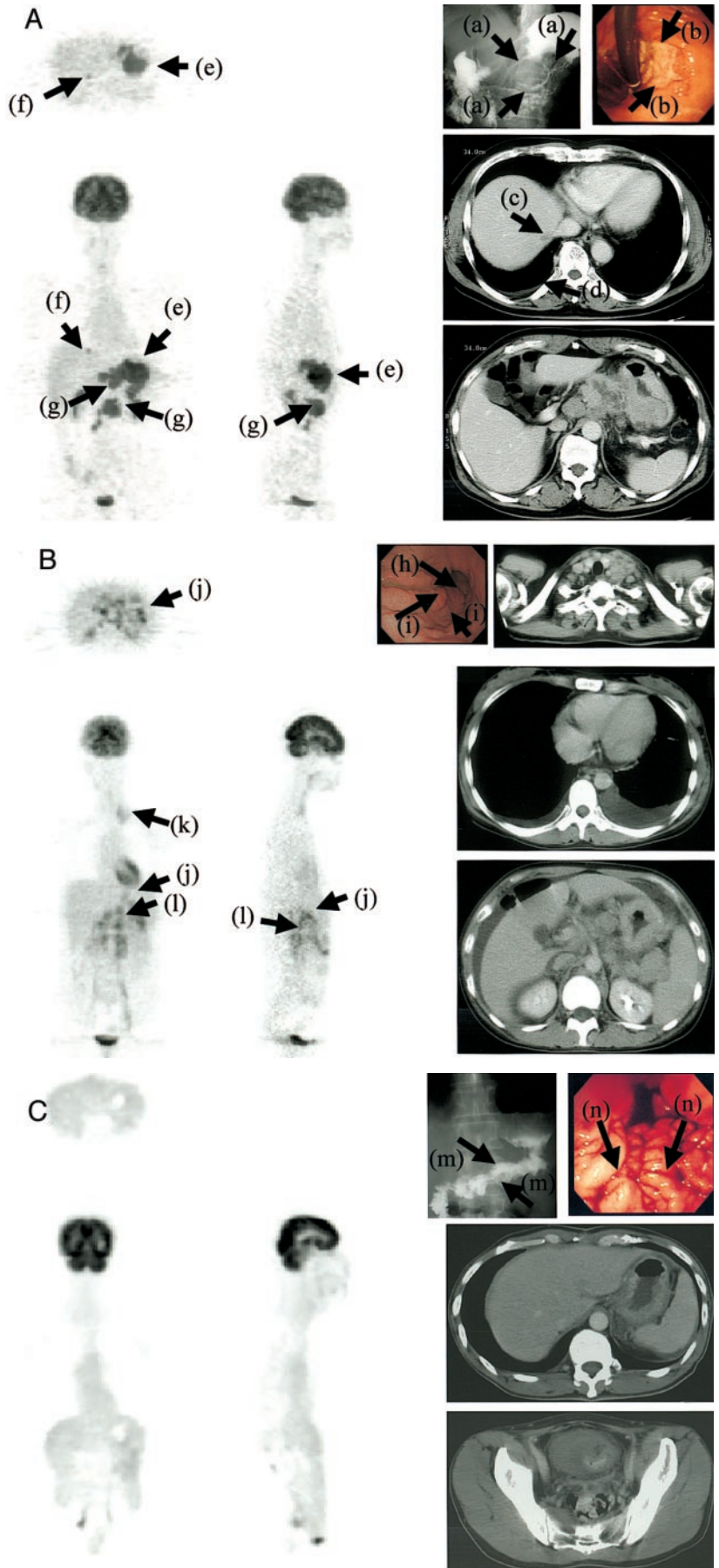


FIGURE 3. Cases with primary lesions. (A) Borrmann type II lesion with liver, lymph node metastases, and pleuritis carcinomatosa (patient S19). Primary lesion is shown as elevated mass with rolled margin on barium radiograph image (arrows, a), accompanying large central ulceration in endoscopic image (arrows, b). Low-density area of 5 mm in diameter in liver (arrow, c) and pleural effusion (arrow, d) are evident on CT image. They have been proven to be liver metastasis and pleuritis carcinomatosa in clinical course. CT image also shows abdominal lymph node metastases. Primary lesion (arrows, e), liver (arrows, f), and abdominal lymph node metastases (arrows, g) are clearly visualized by ^{18}F -FDG PET but pleuritis carcinomatosa is not. (B) Borrmann type III lesion with abdominal, cervical lymph node metastases, and peritonitis and pleuritis carcinomatosa and ascites (patient S15). Endoscopic image shows ulcerated lesion (arrow, h) and infiltration to gastric mucosa (arrows, i). CT images show cervical and abdominal lymph node metastases. They also show pleural effusion and ascites that were diagnosed as malignancy by cytology. Primary lesion (arrows, j), cervical lymph node (arrow, k), and abdominal lymph nodes (arrows, l) are detected by ^{18}F -FDG PET, but no findings indicate peritonitis and pleuritis carcinomatosa or ascites. (C) Borrmann type IV lesion with peritonitis carcinomatosa and ascites (patient S14). Barium radiographic image shows hard wall of stomach without extension (arrows, m), and endoscopic image shows diffusely thickening folds (arrows, n). CT images show thickening wall of stomach and small amount of ascites in pelvis. Patient had undergone exploratory laparotomy that revealed dissemination of small nodal lesions in peritoneum. ^{18}F -FDG PET indicates no findings of Borrmann IV lesion, peritonitis carcinomatosa, or ascites.

each lesion was drawn. Each data point was plotted, changing the degree of the importance of QP and QN to true and false sides.

Quantitative Analysis

Quantitative analysis was performed using image data for the 22 patients who underwent ^{18}F -FDG PET with the SET2400W. The reconstructed image data were converted to the analysis format with the window range of 0–5 SUVs, transferred to the UNIX machine, and analyzed with Doctor View (Mitsubishi Kasei, Co., Japan), a software package that autocalculates SUV maximum, mean, minimum, and SDs by setting the region of interest (ROI). A small circular ROI, 8 mm in diameter (8 or 9 pixels), was used for all patients. Transaxial slices of tomographic images were displayed and ROIs were set on the areas that were thought to be tumors showing high ^{18}F -FDG activity. Adequate numbers of ROIs were sampled from each lesion, and the mean SUV of each ROI was calculated. The maximum mean SUV of tumor areas was recorded as a representative value.

Statistical Analysis

Statistical analysis was performed using the Mann–Whitney *U* test when quantitative results were compared between groups. *P* < 0.05 was considered statistically significant.

RESULTS

Details for macroscopic classification, histology, metastatic sites, and pretreatment as well as patient characteristics are summarized in Table 1. The numbers of patients with primary and secondary lesions are shown in Table 2.

Results of ^{18}F -FDG PET by visual analysis are given in Table 3 and ROC curves are illustrated in Figures 1 and 2. Sensitivity, specificity, and accuracy were 71%, 74%, and 73% for the SET2400W and 47%, 79%, and 62% for the PT931/04 images. They were high for the primary lesions, liver, lymph node, and lung metastases but were low for the

bone metastases, ascites, peritonitis, and pleuritis carcinomatosa (Table 3; Figs. 1 and 2).

Findings for representative cases are shown in Figures 3–5. With regard to macroscopic features of primary lesions, gastric cancers of Borrmann types I, II, and III were readily visible but the Borrmann type IV was not (Fig. 3). Furthermore, in the case classified as Borrmann V (32), for which the tumor was mainly infiltrating diffusely like Borrmann IV, accompanied by ulcerated lesions in part, hot foci of ^{18}F -FDG corresponded only with the ulcer sites (Fig. 4). Liver and lymph nodal metastases could be visualized (Figs. 3A and 3B), but it was difficult to diagnose peritonitis and pleuritis carcinomatosa except where nodal lesions were present on the peritoneal or pleural walls (Fig. 5). Also, it was not easy to detect bone metastases by ^{18}F -FDG PET (Fig. 4).

Quantitative analysis was performed with the image data obtained from 22 patients by the SET2400W. The primary tumors, and metastatic liver, lymph node, abdominal wall, bone, and lung lesions had SUVs of 8.9 ± 4.2 , 6.5 ± 2.2 , 6.1 ± 2.5 , 6.5 ± 1.8 , 3.9 ± 2.0 , and 4.7 ± 2.6 , respectively (Fig. 6). A comparison of values and histologic findings for 17 untreated patients with well-differentiated and moderately to poorly differentiated adenocarcinomas, as well as signet ring cell carcinomas, is given in Table 4. The SUVs for primary lesions and lymph node metastases in the well-differentiated group proved to be higher than those for the poorly differentiated cases, with significance (*P* < 0.05 and *P* < 0.05, respectively) (Table 4).

DISCUSSION

Our study demonstrated the sensitivity, specificity, and accuracy of ^{18}F -FDG PET for primary lesions, liver, lymph

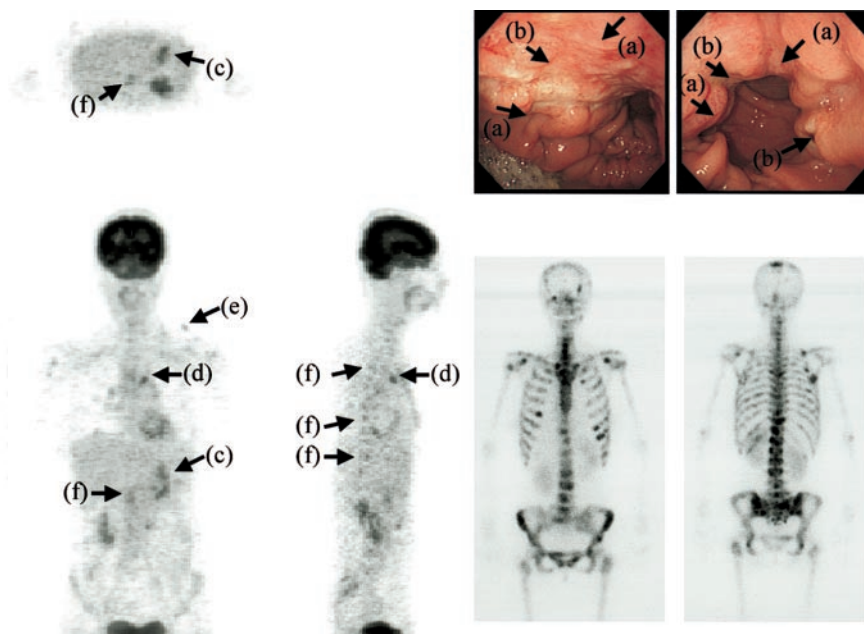


FIGURE 4. Borrmann type V lesions with multiple bone metastases. On endoscopic images, primary lesion is shown as scirrhous infiltration (arrows, a) accompanying some ulcerated areas (arrows, b). ^{18}F -FDG demonstrates hot foci (arrows, c) corresponding to ulcerated areas. On images of bone scintigraphy, there are many hot spots corresponding to metastases on skull, scapula, vertebrae, costae, and sternum, but ^{18}F -FDG PET image suggests bone metastases only in sternum (arrows, d) and part of scapula (arrow, e) and vertebrae (arrows, f).

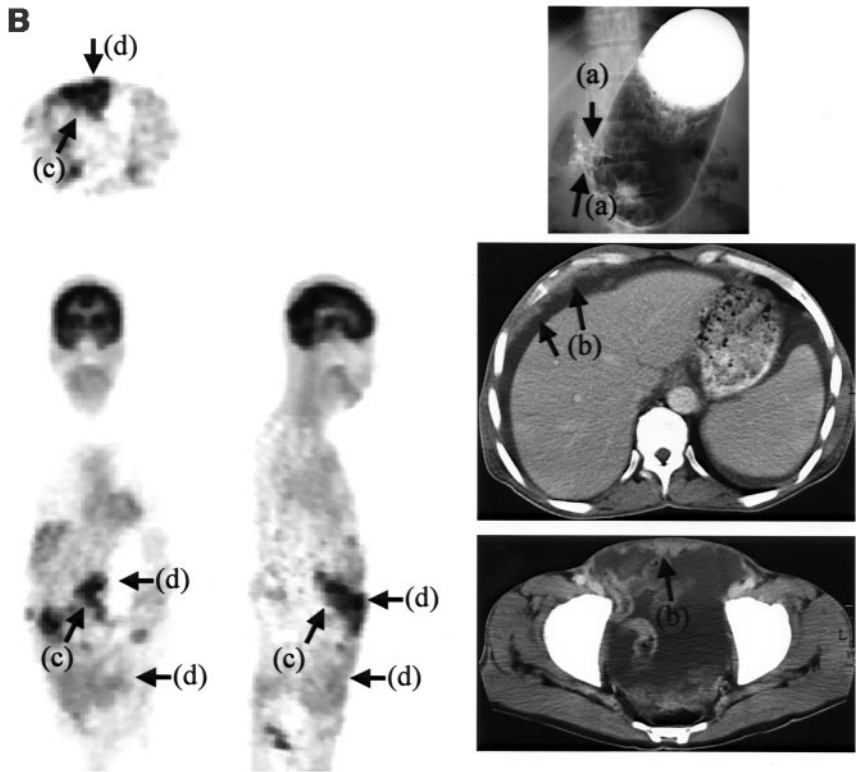
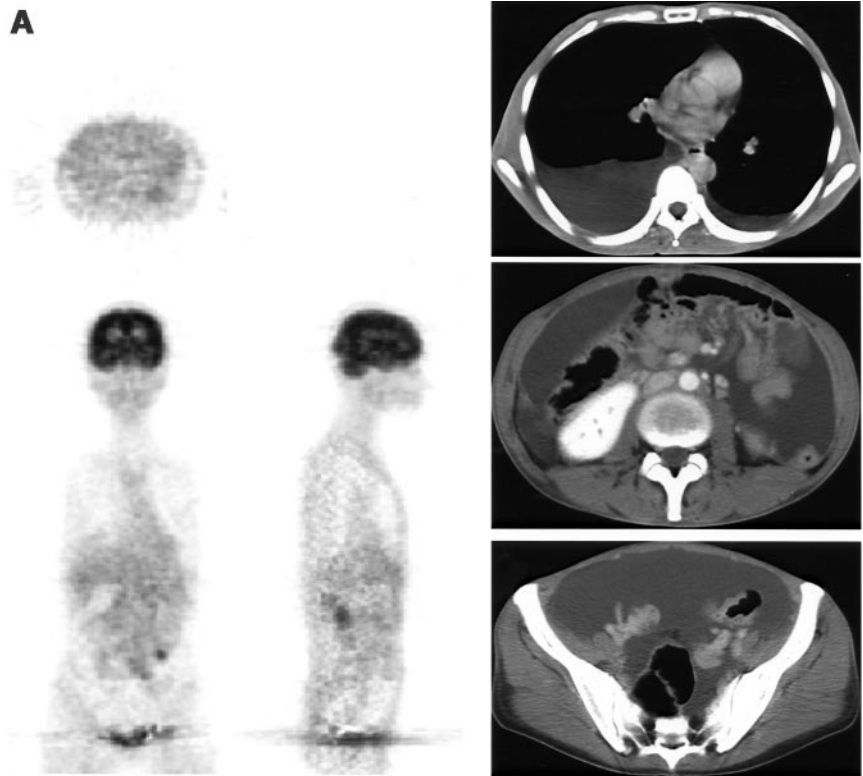


FIGURE 5. Cases with peritonitis or pleuritis carcinomatosa. (A) Recurrence to peritoneal and thoracic cavities after total gastrectomy (patient S09). CT images show large amount of pleural effusion and ascites that were diagnosed as malignancy by cytology, but ^{18}F -FDG PET shows no findings. (B) Borrmann type III lesion with peritonitis carcinomatosa (patient S05). Barium radiographic image shows pyloric stenosis (arrows, a). CT images show large amount of ascites and nodal masses on peritoneal wall (arrows, b). ^{18}F -FDG accumulates in sites corresponding to primary lesion (arrows, c) and nodal masses (arrows, d) on peritoneal wall.

node, and lung metastases to be high, whereas values for ascites, peritonitis, pleuritis carcinomatosa, and bone metastases were low. Detectability was clearly better with the SET2400W than with the PT931/04. We can conclude that

^{18}F -FDG uptake by gastric cancers is relatively high, but without any parallel to the histologic type.

Higashi et al.(17) reported ^{18}F -FDG uptake to reflect the number of viable tumor cells. We speculate that Borrmann

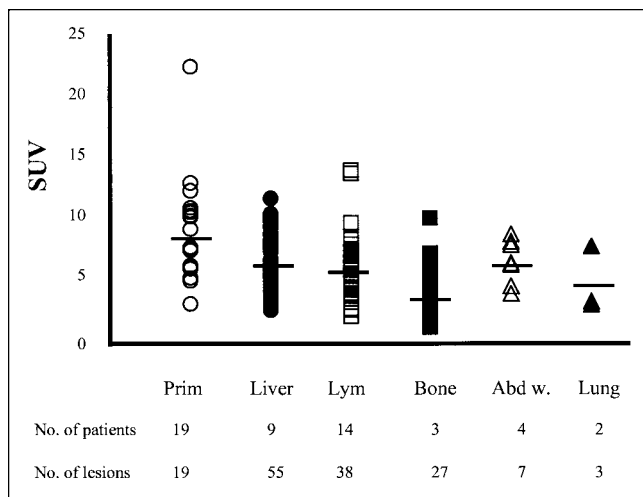


FIGURE 6. SUVs of each lesion. Prim = primary lesions (○); Liver = liver metastases (●); Lym = lymph node metastases (□); Bone = bone metastases (■); Abd w. = abdominal wall tumors (△); Lung = lung metastases (▲). SUVs are 8.9 ± 4.2 , 6.5 ± 2.2 , 6.1 ± 2.5 , 3.9 ± 2.0 , 6.5 ± 1.8 , and 4.7 ± 2.6 , respectively. SUVs of primary lesions, liver, and lymph node metastases involve data from 2 patients who had prior chemotherapy. SUVs from patients who were chemotherapy naive are given in Table 4. SUVs of bone, abdominal wall, and lung metastases are all from patients who were chemotherapy naive.

types I, II, and III are easily visible because the malignant cells are densely packed, whereas with the Borrmann type IV they infiltrate into the gastric wall with much intermingled stromal tissue. Regarding the tumor that was infiltrating diffusely, accompanied by ulcerated lesions in part, the fact that hot foci of ^{18}F -FDG corresponded with the ulcerated sites (Fig. 4) is in line with the report of Kubota et al. (33) that macrophages and granulation tissues demonstrate marked accumulation of ^{18}F -FDG.

The sensitivity, specificity, and accuracy of ^{18}F -FDG PET for liver, lymph node, and lung metastases were here found to be high. The smallest lesion detected by ^{18}F -FDG PET

was a liver metastasis of 0.5 cm in diameter in patient S19 (Fig. 3A), and ^{18}F -FDG PET for metastatic lesions in nodes appears to be reliable. However, in our study, ^{18}F -FDG PET did not detect locoregional lymph node metastases. Lerut et al. (34) reported that the regional lymph node metastases were not detected with high accuracy, in line with findings of our study. On the other hand, no ^{18}F -FDG PET images revealed the existence of malignant ascitic fluid or pleural effusion (Fig. 5A). In patients E06, E13, S03, S11, and S14, dissemination of small nodal lesions in the peritoneum was confirmed by previous palliative surgery, but they were not detected by ^{18}F -FDG PET and the diagnosis of peritonitis or pleuritis carcinomatosa was possible only when deposits were present on the peritoneal or pleural wall (Fig. 5B) and their sizes were >2 cm in diameter. Potter et al. (28) reported earlier that ^{18}F -FDG PET was not suited for screening purposes in the follow-up of treated gastric cancer because of its moderate accuracy. They pointed to incorrect PET diagnoses of recurrent gastric cancers caused by peritoneal metastases, in line with our study findings. We speculate that ^{18}F -FDG exudes from vessels into the peritoneal or thoracic cavity and the actual concentrations may be very low. If possible, ascitic fluid or pleural effusion should be examined for ^{18}F -FDG activity.

Our study group included 3 patients with bone metastases (Fig. 4), suspected on the basis of hypercalcemia, hyperalkaline phosphatase, or bone pain, for which $^{99\text{m}}\text{Tc}$ -MDP bone scintigraphies were performed. The number of bone metastases detected with ^{18}F -FDG PET was fewer than that with bone scanning. ^{18}F -FDG PET appears to be superior to bone scintigraphy at detecting bone metastases from lymphomas (35) and breast cancers (36) but is disappointing with prostate cancer (37). Cook et al. (38) reported that ^{18}F -FDG PET gave more accurate results than scintigraphy for osteolytic but not osteoblastic breast cancer metastases. They speculated that osteoblastic metastases might be acellular with low volumes of viable tumor. In addition, osteo-

TABLE 4
Comparison of SUVs Between Different Histologic Types

Primary lesions or metastases	Overall		Untreated		Well + mod		Poor + sig	
	No.*	SUV	No.*	SUV	No.*	SUV	No.*	SUV
Prim	19 (19)	8.8 ± 4.2	17 (17)	9.0 ± 4.3	4 (4)	13.2 ± 6.3	13 (13)	7.7 ± 2.6
Liver	9 (55)	6.5 ± 2.2	7 (41)	6.9 ± 2.4	2 (2)	5.6 ± 2.8	5 (39)	7.0 ± 2.4
Lym	14 (38)	6.1 ± 2.5	12 (36)	6.2 ± 2.6	3 (8)	8.8 ± 3.2	9 (28)	5.5 ± 1.9

$P < 0.05$ (between Well + mod and Poor + sig for Prim, Liver, and Lym)

*No. = no. of patients (no. of lesions).
 Overall = all lesions; Untreated = untreated lesions; Well = well-differentiated adenocarcinoma; mod = moderately differentiated adenocarcinoma; Poor = poorly differentiated adenocarcinoma; sig = signet ring cell carcinoma; Prim = primary lesions; Liver = liver metastases; Lym = lymph node metastases.
 P value; Mann-Whitney U test.

lytic lesions might be expected to outstrip their blood supply, which renders them hypoxic, and this might increase ^{18}F -FDG uptake. In our patients, obviously osteolytic lesions evident on radiography were also detected by ^{18}F -FDG PET, but the osseous lesions with no clear changes on plain bone radiographs were missed. Small numbers of malignant cells might induce an osteoblastic response to bone metastases from gastric cancers and, therefore, $^{99\text{m}}\text{Tc}$ -MDP bone scintigraphy might be superior to ^{18}F -FDG PET for their detection. However, because our study covered only 3 cases, further investigations are needed for confirmation.

In the present comparison, the SET2400W was clearly superior to the PT931/04 (Table 3). This is due to the differences of machine performances, involving the special resolution. But the postinjection transmission technique also improved the results. ^{18}F -FDG is trapped and converted to ^{18}F -FDG-6-phosphate in the liver, dephosphorylated by a key enzyme for gluconeogenesis, and excreted (3). The later the emission scan starts after ^{18}F -FDG injection, the better the signal-to-noise ratio for liver metastasis. With the PT931/04, patients had to wait on the bed of the scanner from the start of the transmission to the end of the emission and maintain the same supine position. Because this inflicts pain on individuals suffering from severe disease, the total time of the examination must be kept as short as possible. With the SET 2400W, the use of postinjection transmission removes this limitation. Because patients can relax after the injection for the examination, the period after the injection to emission scanning can be lengthened.

Our quantitative analysis revealed the SUVs for gastric cancers to be relatively elevated compared with other kinds of cancer (5–16). Primary lesions, liver and lymph node metastases, as well as abdominal nodal metastases, demonstrated higher values than bone metastases. The SUVs for highly differentiated types were significantly greater than with poorly differentiated types of primary lesions and lymph node metastases. Stahl et al. (27) reported mucinous and signet ring cell carcinomas to show significantly lower ^{18}F -FDG uptake than other histologic types of gastric cancer. These results contrast with our previous findings using human xenografts that ^{18}F -FDG uptake increases with loss of differentiation (39). However, in the latter, the volume ratios of tumor parenchyma to stroma were almost the same among all human xenografts. Poorly differentiated adenocarcinomas and signet ring cell carcinomas tend to infiltrate into the gastric wall with much stromal tissue, whereas well-differentiated and moderately differentiated adenocarcinomas form tumor masses. We speculate that low ^{18}F -FDG accumulation in poorly differentiated types of primary lesions, in spite of their aggressiveness, occurs because of the low concentration of cancer cells. The same might be expected to occur with lymph node metastases, but it is well known that the degree of differentiation of primary and metastatic lesions with gastric cancers can be very different. We conclude that further investigations are needed to com-

pare ^{18}F -FDG uptake and the histologic appearance of metastatic lesions.

Recently, response evaluation criteria in solid tumors have been widely applied for evaluation of cancer treatment (40). This method is based on helical CT but ignores the efficacy with regard to the primary lesion because it cannot be measured with the approach in gastric cancer cases. Our study revealed that ^{18}F -FDG PET can detect and evaluate semiquantitatively primary lesions other than with Borrmann type IV disease, as well as major metastatic sites, and, therefore, could be used as an instrument for assessing treatment, especially chemotherapy. However, ^{18}F -FDG PET may fail to detect primary lesions of Borrmann type IV, peritonitis, pleuritis carcinomatosa, and bone metastases, despite those being high-grade malignancy. In the application of ^{18}F -FDG PET for gastric cancer, attention thus should be paid to the risk of missing important lesions.

CONCLUSION

Our study indicates that ^{18}F -FDG PET is a useful diagnostic modality for advanced, metastatic, or recurrent gastric cancers but may have difficulty in detecting peritoneal and pleural carcinomatoses and bone metastases. ^{18}F -FDG uptake of primary or metastatic gastric cancers is comparatively high but does not necessarily parallel the grade of malignancy.

ACKNOWLEDGMENTS

The authors thank Drs. Hirotsuke Oikawa and Syunich Maeda for their help with collection of PT931/04 images; Syouichi Watanuki, Yasushi Miyake, and Norihiko Seo for PET operation; and Professor Hikonojyo Orihara and the staff of the Cyclotron and Radioisotope Center, Tohoku University, for their assistance. We also thank Dr. Malcolm Moore for reading and editing the manuscript. This work was supported by Grants-in-Aid for Scientific Research (13670910 and 10670820) from the Ministry of Education, Science, Sports, Culture, and Technology and for Cancer Research (11S-3) from the Ministry of Health, Labor, and Welfare, Japan.

REFERENCES

1. Cancer Statistics in Japan '01. Available at: <http://www.ncc.go.jp/en/statistics/2001/index.html>. Accessed July 1, 2002.
2. Reivich M, Kuhl D, Wolf A, et al. The [^{18}F]fluorodeoxyglucose method for the measurement of local glucose utilization in man. *Circ Res*. 1979;44:127–137.
3. Gallagher BM, Fowler JS, Gutters NI, MacGregor RR, Wan CN, Wolf AP. Metabolic trapping as a principle of radiopharmaceutical design: some factors responsible for the biodistribution of [^{18}F]2-deoxy-2-fluoro-D-glucose. *J Nucl Med*. 1978;19:1154–1161.
4. Warburg O. On the origin of cancer cells. *Science*. 1956;123:309–314.
5. Kubota K, Matsuzawa T, Fujiwara T, et al. Differential diagnosis of lung tumor with positron emission tomography: a prospective study. *J Nucl Med*. 1990;31:1927–1933.
6. Kubota K, Yamada S, Kondo T, et al. PET imaging of primary mediastinal tumours. *Br J Cancer*. 1996;73:882–886.
7. Lindholm P, Leskinen-Kallio S, Minn H, et al. Comparison of fluorine-18-fluorodeoxyglucose and carbon-11-methionine in head and neck cancer. *J Nucl Med*. 1993;34:1711–1716.

8. Avril N, Dose J, Janicke F, et al. Metabolic characterization of breast tumors with positron emission tomography using F-18 fluorodeoxyglucose. *J Clin Oncol.* 1996;14:1848–1857.
9. Lapela M, Leskinen S, Minn HRI, et al. Increased glucose metabolism in untreated non-Hodgkin's lymphoma: a study with positron emission tomography and fluorine-18-fluorodeoxyglucose. *Blood.* 1995;86:3522–3527.
10. Fukunaga T, Okazumi S, Koide Y, Isono K, Imazeki K. Evaluation of esophageal cancers using fluorine-18-fluorodeoxyglucose PET. *J Nucl Med.* 1998;39:1002–1007.
11. Abdel-Nabi H, Doerr RJ, Lamonica DM, et al. Staging of primary colorectal carcinomas with fluorine-18-fluorodeoxyglucose whole-body PET: correlation with histopathologic and CT findings. *Radiology.* 1998;206:755–760.
12. Delbeke D, Rose DM, Chapman WC, et al. Optimal interpretation of FDG PET in the diagnosis, staging and management of pancreatic carcinoma. *J Nucl Med.* 1999;40:1784–1791.
13. Torizuka T, Tamaki N, Inokuma T, et al. In vivo assessment of glucose metabolism in hepatocellular carcinoma with FDG-PET. *J Nucl Med.* 1995;36:1811–1817.
14. Sugawara Y, Eisbruch A, Kusuda S, Recker BE, Kison PV, Wahl RL. Evaluation of FDG PET in patients with cervical cancer. *J Nucl Med.* 1999;40:1125–1131.
15. Effert PJ, Bares R, Handt S, Wolff JM, Bull U, Jakse G. Metabolic imaging of untreated prostate cancer by positron emission tomography with ¹⁸F-fluorine-labeled deoxyglucose. *J Urol.* 1996;155:994–998.
16. Gritters LS, Francis IR, Zasadny KR, Wahl RL. Initial assessment of positron emission tomography using 2-fluorine-18-fluoro-2-deoxy-D-glucose in the imaging of malignant melanoma. *J Nucl Med.* 1993;34:1420–1427.
17. Higashi K, Clavo AC, Wahl RL. Does FDG uptake measure proliferative activity of human cancer cells? in vivo comparison with DNA flow cytometry and tritiated thymidine uptake. *J Nucl Med.* 1993;34:414–419.
18. Abe Y, Matsuzawa T, Fujiwara T, et al. Assessment of radiotherapeutic effects on experimental tumors using ¹⁸F-2-fluoro-2-deoxy-D-glucose. *Eur J Nucl Med.* 1986;12:325–328.
19. Yoshioka T, Takahashi H, Oikawa H, et al. Influence of chemotherapy on FDG uptake by human cancer xenografts in nude mice. *J Nucl Med.* 1997;38:714–717.
20. Abe Y, Matsuzawa T, Fujiwara T, et al. Clinical assessment of therapeutic effects on cancer using ¹⁸F-2-fluoro-2-deoxy-D-glucose and positron emission tomography: preliminary study of lung cancer. *Int J Radiat Oncol Biol Phys.* 1990;19:1005–1010.
21. Wahl RL, Zasadny K, Helvie M, et al. Metabolic monitoring of breast cancer chemohormonotherapy using positron emission tomography: initial evaluation. *J Clin Oncol.* 1993;11:2101–2111.
22. Haberkorn U, Strauss LG, Dimitrakopoulou A, et al. Fluorodeoxyglucose imaging of advanced head and neck cancer after chemotherapy. *J Nucl Med.* 1993;34:12–17.
23. Ichiya Y, Kuwabara Y, Otsuka M, et al. Assessment of response to cancer therapy using fluorine-18-fluorodeoxyglucose and positron emission tomography. *J Nucl Med.* 1991;32:1655–1660.
24. Couper GW, McAteer D, Wallis F, et al. Detection of response to chemotherapy using positron emission tomography in patients with oesophageal and gastric cancer. *Br J Surg.* 1998;85:1403–1406.
25. MacAteer D, Wallis F, Couper G, et al. Evaluation of ¹⁸F-FDG positron emission tomography in gastric and oesophageal carcinoma. *Br J Radiol.* 1999;72:525–529.
26. Kole AC, Plukker JT, Nieweg OE, Vaalburg W. Positron emission tomography for staging of oesophageal and gastroesophageal malignancy. *Br J Cancer.* 1998;78:521–527.
27. Stahl A, Ott K, Weber WA, Fink U, Siewert JR, Schwaiger M. Correlation of FDG uptake in gastric carcinomas with endoscopic and histopathological findings [abstract]. *J Nucl Med.* 2001;42(suppl):78P.
28. Potter TD, Flamen P, Cutsem EV, et al. Whole-body PET with FDG for the diagnosis of recurrent gastric cancer. *Eur J Nucl Med.* 2002;29:525–529.
29. Shiue CY, Salvadori PA, Wolf AP, Fowler JS, MacGregor RR. A new improved synthesis of 2-deoxy-2-[¹⁸F]fluoro-D-glucose from ¹⁸F-labeled acetyl hypofluorite. *J Nucl Med.* 1982;23:899–903.
30. Watanuki S, Ishii K, Orihara H, Fukuda H, Matsuzawa T. Status of multi-ring high-resolution positron emission tomography system PT931. *CYRIC Annual Report.* Sendai, Japan: Cyclotron Center, Tohoku University; 1986:240–244.
31. Fujiwara T, Watanuki S, Yamamoto S, et al. Performance evaluation of a large axial field-of-view PET scanner: SET-2400W. *Ann Nucl Med.* 1997;11:307–313.
32. Japanese Gastric Cancer Association. *Japanese Classification of Gastric Carcinoma.* 13th ed. Tokyo, Japan: Kanehara & Co.; 1999:4–13.
33. Kubota R, Yamada S, Kubota K, Ishiwata K, Tamahashi N, Ido T. Intratumoral distribution of fluorine-18-fluorodeoxyglucose in vivo: high accumulation in macrophages and granulation tissues studied by microautoradiography. *J Nucl Med.* 1992;33:1972–1980.
34. Lerut T, Flamen P, Ectors N, et al. Histopathologic validation of lymph node staging with FDG-PET scan in cancer of the esophagus and gastroesophageal junction: a prospective study based on primary surgery with extensive lymphadenectomy. *Ann Surg.* 2000;232:743–752.
35. Moog F, Kotzerke J, Reske SN. FDG PET can replace bone scintigraphy in primary staging of malignant lymphoma. *J Nucl Med.* 1999;40:1407–1413.
36. Moon DH, Maddahi J, Silverman DHS, Glaspy JA, Phelps ME, Hoh CK. Accuracy of whole-body fluorine-18-FDG PET for the detection of recurrent or metastatic breast carcinoma. *J Nucl Med.* 1998;39:431–435.
37. Shreve PD, Grossman HB, Gross MD, Wahl RL. Metastatic prostatic cancer: initial findings of PET with 2-deoxy-2-[F-18]fluoro-D-glucose. *Radiology.* 1996;199:751–756.
38. Cook GJ, Houston S, Rubens R, Maisey MN, Fogelman I. Detection of bone metastases in breast cancer by ¹⁸F-FDG PET: differing metabolic activity in osteoblastic and osteolytic lesions. *J Clin Oncol.* 1998;16:3375–3379.
39. Yoshioka T, Takahashi H, Oikawa H, et al. Accumulation of 2-deoxy-2-[¹⁸F]fluoro-D-glucose in human cancers heterotransplanted in nude mice: comparison between histology and glycolytic status. *J Nucl Med.* 1994;35:97–103.
40. Therasse P, Arbuck SG, Eisenhauer EA, et al. New guidelines to evaluate the response to treatment in solid tumors. *J Natl Cancer Inst.* 2000;92:205–216.